Machine Learning-based optimization and PIV analysis of the active control of a cylinder wake via synthetic jets

Alessandro Scala[1*]

[1*]Department of Industrial Engineering, University of Naples "Federico II", via Claudio 21, Naples, 80125, Italy.

Corresponding author(s). E-mail(s): alessandro.scala2@unina.it;

Abstract

The aim of the present paper is the investigation of the Synthetic Jet (SJ) based control of a cylinder wake through Linear Genetic Programming (LGP) technique and the flow field via Particle Image Velocimetry (PIV) technique. Machine Learning is a branch of Artificial Intelligence aimed at extracting knowledge and experience from big volumes of data and it is the art of building models from data using optimization and regression algorithms. A SJ is an actuator used mainly for flow control and heat transfer performances. In this work, a loudspeaker attached to an hollow cylinder is used as SJ actuator device and the optimization procedure regards the input signal sent to the device. A gradient-enriched machine learning control, know as gMLC algorithm, is used as optimization tool. A preliminary phase of analysis of the ML algorithm, in which an optimal control law is found, is conducted. The latter allows to obtain a very complex control law which is able to give a percentage drag reduction of 7.6 % with respect to the natural case and this reduction is found to be better than the one obtained by a reference sinusoidal signal characterized by a fundamental frequency of 44 Hz. After the ML analysis, an investigation via Particle Image Velocimetry is performed with the aim of of obtaining a comparison between the natural case, i.e. the uncontrolled configuration, and two different controlled cases: the optimal waveshape obtained via gMLC algorithm and the previous-mentioned sinusoidal waveshape.

Keywords: Machine Learning, Particle Image Velocimetry, Active Flow Control

1 Introduction

In the few last years, the relationship between Machine Learning (ML) and fluid dynamics has become more and more important. Machine learning is the art of building model from data using optimization and regression algorithms and many of the challenges in fluid dynamics may be posed as optimization problems, such as designing a wing to maximize the lift while minimizing the drag at the cruise velocities or simply minimizing the drag of a cylinder wake. These optimization tasks fit well with machine learning algorithms, which are designed to handle nonlinear and high-dimensional problems, such as the one which would be widely later discussed, i.e. the control of cylinder's wake via Synthetic Jets (SJ).

Flow control has always been a research topic of great interest for the entire scientific community. In the field of flow manipulation, the control of the wake of bluff bodies, characterized by the vortex shedding phenomenon, has a great relevance and especially, the wake of the circular cylinder and the possibility of controlling it, have attracted a large amount of research due to their importance in all aspects of engineering applications.

Vortex shedding from a single circular cylinder, develops over a wide range of Reynolds number $Re = DU_\infty/\nu$ (with D being the circular cylinder diameter, U_∞ the free-stream velocity and ν the fluid kinematic viscosity) starting from a critical value ($Re \approx 49$) above which the laminar symmetric bubble behind the body becomes unstable. This phenomenon is due to a wake instability associated with a rather sudden inception and growth in amplitude of wake fluctuations, as one increases the Reynolds number [1].

Various strategies have been adopted to control and prevent the von Kármán shedding and these can be divided into two different groups: passive and active flow control. The category of active flow control includes synthetic jets which have been proven to be an efficient flow control technique thanks to their advantageous features, such as reduced size and weight, improved manufacturability, low cost and high reliability [2].

A conventional synthetic jet device consists of a cavity bounded on one side by a membrane (such as a piezoelectric or loudspeaker) and on the opposite side by a slot/circular exit. The essential characteristic of the synthetic jet is that it can generate vortical structures, i.e., vortex pairs or vortex rings periodically from the orifice. Indeed, the fluid is periodically ejected and sucked from the orifice by the periodic motion of the driving membrane bounding the synthetic jet device cavity. These jets are zero-net-mass- flux in nature; indeed, they are 'synthesized' from the ambient fluid in which the device is embedded [3].

Previous works (e.g., [2],[4]) have analysed the performance of a synthetic jet-based control of a cylinder wake considering the variation of two control parameters, generally the momentum coefficient and the dimensionless frequency. On the other side, few attempts have been made to evaluate the effects of the input signal shape. [5]. In the latter works, the signal waveshape was however defined in a parametric way (sinusoidal signals with varying suction duty cycle were investigated).

Mathematically, the flow control problem can be studied as a functional optimization problem, in which the state of the dynamical system has to be inferred from a limited number of observable quantities. The objective is to find a control function that minimizes (or maximizes) a cost (or reward) function, based on the desired characteristics for the controlled flow configuration. In the recent years, Machine Learning has found its way in the application of AFC and especially in the model-free control techniques where an optimized control law is extracted without imposing any model of the dynamical system. In this framework, one the most prominent model-free technique used is the Linear Genetic Programming (LGP).

In the present study, LGP algorithms are used to overcome the limitations inherent to the assumption of a parametric waveshape and to find the optimal waveshape of the input signal for the drag reduction of the cylinder body.

The gradient-enriched machine learning control (gMLC) algorithm developed by Maceda et al. [6] has been chosen as optimization tool to find the best open-loop control law in terms of the input voltage signal with respect to the time of actuation. The gMLC control law obtained also seems to be different from others reported in several studies in literature; in fact, it appears to be a sinusoidal waveshape which tends to a square wave. Such an optimal waveshape has been compared with a sinusoidal reference signal to show differences in aerodynamic drag reduction.

Starting from this identified optimal waveshape, the use of PIV allows to obtain instantaneous two-dimensional in-plane velocity fields measurements in a plane containing the synthetic jet slot and these have been used to investigate the mean flow quantities and turbulent statistics of the phenomenon. Such an analysis allows to observe major differences between controlled configurations not specifically on the time-averaged flow fields where such differences between gMLC control law and sinusoidal control law do not emerge, but especially on the fluctuating fields for the velocity components. In fact, looking at the Reynolds stress and Turbulent kinetic energy maps, it is possible to infer that gMLC actuation law is able to reduce the velocity fluctuations in the wake better than the sinusoidal control law. This can be translated into a better suppression of the vortex shedding phenomenon in the case of gMLC control law compared with sinusoidal waveshape. In addition, modal decomposition performed on PIV input data via Proper Orthogonal Decomposition (POD) has been executed to better analyze the interaction between the SJ and the cylinder's wake to understand the variation of characteristic modes of the flow field with the application of SJ control.

2 Experimental Setup

The experiments are carried out in the subsonic open circuit wind tunnel available at the Experimental Thermo-Fluid Dynamic Laboratory of the University of Naples "Federico II" and sketched in Figure 1, where all the components

involved during the experimental analysis are reported. The subsonic open-circuit wind tunnel employed in the experiments has got a rectangular test section of 300 mm × 400 mm. The tunnel inlet nozzle has a contraction ratio of 10 which ensures a low turbulence intensity (0.1 %) in the test section. The flow is seeded with nebulized olive oil, with particles diameter of approximately 1 μm, by means of a Laskin nozzle seeding generator. Such a generator is connected to a seeding rake, which is positioned close to the wind tunnel inlet and allows to obtain a uniform seeding of the test section. The wind tunnel is operated at a free-stream velocity $U_\infty = 10.3\ ms^{-1}$, as also measured by PIV.

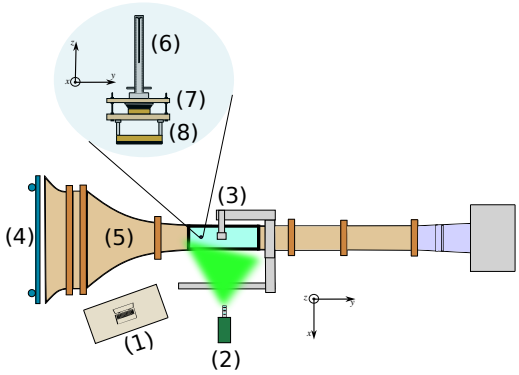

Fig. 1 Schematic representation of the experimental setup. The experimental setup components reported are: Computer Station and Arduino Card (1), Low-speed Laser (2), Acquisition Camera (3), Laskin Nozzle and seeding rake (4), Subsonic wind tunnel (5), hollow circular cylinder (6), Loudspeaker (7), load cells (8).

The test body is an hollow cylinder (6) whose axis is centered on the 400 mm side of the wind tunnel test section and it is 400 mm downstream of the convergent nozzle end. The hollow cylinder inner and outer diameters are 24 and 30 mm, respectively. Such a body is coupled with a loudspeaker (7) driven by an electrical signal which is generated using a wave generator coupled with a four-channel power amplifier. Thanks to the vibration of the loudspeaker, the fluid is periodically ejected and sucked from a slot placed on the cylinder surface, at the rear stagnation point, generating the synthetic jet. The slot is placed on the cylinder surface with a width $h = 0.8$ mm and a length $l = 270$ mm. A Sensirion SDP1000-L025 differential pressure transducer is used to measure the dynamic pressure in the inlet nozzle of the wind tunnel with the purpose of computing the free stream velocity U_∞ in the test section, whilst a couple of load cells (8), placed under the cylinder, are employed for measuring the cylinder aerodynamic drag. All the signals from these sensors are sent to an Arduino One board which is appointed to acquire all the measurements. The wind tunnel facility is equipped with a planar PIV system used to carry out velocity measurements of the wake in a plane orthogonal to the cylinder

axis. Such a system consists of a Quantel Evergreen low-speed laser (2), Nd-YAG, 200 mJ/pulse, and a Andor Zyla 5.5 mega-pixels sCMOS camera (3) equipped with a 50 mm focal length lens, thus obtaining a resolution of 24.85 pixel mm^{-1}.

3 Machine Learning Procedure

For flow control problems, LGP can be considered as a powerful regression technique able to re-discover and combine different flow control strategies, which have been proven useful in the cases of multi-frequency forcing or direct feedback control. In AFC based on LGP, the control laws are often named as *individuals* to match with the evolutionary terminology. Linear Genetic Programming is able to learn control laws in a model-free manner, optimizing both the structure of the function and its parameters. In practice, the control laws are internally represented by a matrix encoding a list of instructions. Each row of the matrix codes for a mathematical operation from a set of input registers, constants and operations and stores the result in a memory register. The matrix is then read linearly modifying sequentially the memory registers.

Recently, an improved faster version of Machine Learning Control (MLC) based on the addition of intermediate gradient-descent steps between the generations (gMLC) has been developed by Maceda et al. in their work [6].

The gMLC procedure differs from MLC in two principal aspects. First, the concept of evolution from generation to generation is not adopted. The genetic operations include all tested individuals. Second, the exploitation is accelerated by downhill subplex iteration [7]. Indeed, gMLC enhances model-free control optimization combining the advantages of both exploitation and exploration. Exploitation is based on the downhill simplex method just mentioned and the goal of this phase is to 'slide down' the best identified minimum, while exploration phase is performed with LGP algorithm using all previously tested individuals. The goal is to find potentially new and better minima, ideally the global minimum; this task is carried out by the LGP algorithm.

The algorithm starts with the a random generation of an initial population of N_{MC} individuals evaluated with a Monte-Carlo optimization to explore the control law space. A measure of the performance of each individual is given by its cost J. Once the initial population is evaluated, new individuals are created thanks to genetical operations (crossover, mutation and replication) applied to the most performing individuals. A tournament selection of size 7 for a population of 100 individuals is used in the work by Maceda et al. [6], as done also by Duriez et al. [8]. This means that for a population of 100 individuals, 7 individuals are selected randomly and among the 7, the best one is chosen for the crossover or mutation operation. Once achieved the evolution phase, a new set of individuals is succesfully generated thanks to downhill subplex iterations. For this particular application, Maceda et alt. proposed a different version of the Nelder-Mead algorithm based on the one developed by Rowan [7]. To limit the number of cost function evaluations, the downhill simplex

has been applied only to one subspace. The learning process is repeated for every new generation until the stopping criterion is met or if the termination is triggered.

For our experiments, we decided to consider a number of initial control laws N_{MC} equal to 100. These control laws have been generated combining an initial set of twelve harmonic functions with fundamental frequency of 44 Hz, moving up to 264 Hz and leaving the algorithm free to explore the possibility of combining these laws using several operations and operators(i.e. sum, difference, multiplication and application of mathematical operators such as sine and cosine functions). The choice of a such fundamental frequency derives from a previous experimental parametric investigation. It should also be pointed out that the phase of combining the control laws is not bound to obtaining periodic control laws, but could also obtain constant control laws which, however, would be discarded by the algorithm in the process of selecting the best individuals.

The control problem is formulated as a regression problem, i.e. to find the control law which optimizes a given cost function. A critical choice in the process is linked to the definition of the proper cost function J specified for this optimization problem. In our study, we adopted a simplified cost function law J defined as follows :

$$J = 1 + C_D - C_{D_B} \tag{1}$$

where C_D represents the instantaneous drag coefficient value measured by load cells while C_{D_B} is the baseline drag coefficient value measured in the uncontrolled configuration. Therefore, this cost function expression is based on the increment with respect to the unforced flow which is intended to be as negative as possible.

The most relevant parameters for a proper performance and convergence of the gMLC algorithm are the population size, the number of generations, the tournament selection size and the genetic operators' probability (P_c, P_m, P_r) which are reported, for the case in exam, in the following table.

Table 1 LGPC parameters

Number of Actuators	1
Population size	100
Montecarlo Population size	100
Number of generations	15
Tournament selection size	7
Crossover probability	0.6
Mutation probability	0.3
Replication probability	0.1
Elitism	1
Operations	$+, -, \times, \sin, \cos, \tanh$

4 Data Reduction and analysis

As regards the PIV measurements, the vector field is obtained by pre-processing the images through background noise removal algorithm and then processing them with a multiple-pass algorithm with image deformation using Blackman weighting windows, according to Astarita [9, 10]. 2-D component PIV measurements are performed with an acquisition frequency of 10 Hz corresponding to a sequence of 2000 snapshots for each of the cases studied.

Proper Orthogonal Decomposition (POD) is used to analyze and decompose the velocity field starting from the raw data obtained by means of PIV technique.

The proper orthogonal decomposition is a statistical method based on the extraction of a basis for modal decomposition from an ensemble of signals [11]. POD allows to obtain a linear decomposition of the available signals, which, among all the linear decompositions, is optimal from an energetic point of view. Such a feature has made it become a fundamental tool in the analysis of complex turbulent flows, often preferable to other techniques because of the simple and clear interpretation to which POD modes are prone. POD generally allows for identification of the most energetic coherent structures, which play a crucial role in various engineering applications like mixing, heat transfer, generation of aerodynamic forces, etc.. General scheme of application of POD to a specific fluid mechanics problem is reported in Figure 2.

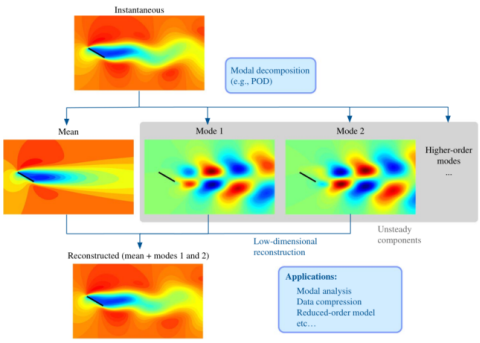

Fig. 2 Modal decomposition of two-dimensional incompressible flow over a flat-plate wing. This example shows complex nonlinear separated flow being well represented by only two POD modes and the mean flowfield. (from Taira et al.[12])

Such a modal analysis technique was introduced to the fluid dynamics/turbulence community by pioneering work written by Lumley [13] as a mathematical technique to extract coherent structures from turbulent flowfields. However, this technique was independently formulated by different scientists some years before and, in other contexts, it is also known as Karhunen–Loève decomposition or principal component analysis. The mathematical foundation of POD is provided by the spectral theory of compact

self-adjoint operators, which applies to both discrete and continuous signals. A general mathematical presentation of such a theory goes beyond the scope of the present dissertation, but the interested reader can find a deeper dissertation in [14, 15].

5 Results and discussion

The main goal of the current work is to seek for an optimal control strategy provided by linear genetic programming. Initially, a preliminary phase of exploration of the physical domain in uncontrolled environment has been performed. Then, the gMLC algorithm has been applied with the aim of searching for an optimal wave shape which could lead to a drag coefficient best reduction. At the end, an investigation involving also a sinusoidal waveshape has been performed with the aim of comparing the control performance obtained using LGP with the one obtained considering a waveshape widely used in literature. On the mentioned control configurations, Particle Image Velocimetry measurements have been performed to obtain instantaneous two-dimensional in-plane velocity fields in a plane containing the synthetic jet slot and these have been used to investigate the mean flow quantities and turbulent statistics of the phenomenon.

5.1 Linear Genetic Programming Procedure

As previously mentioned, an adaptation of the gMLC algorithm [6] has been developed, modifying such an algorithm for the specific optimization problem in exam. Since the cost function expression is dependent from the baseline drag coefficient value (i.e. the uncontrolled drag coefficient), a preliminary analysis in a no-control environment has been performed. Such an investigation showed a value for the C_{D_B} equals to 0.91, for a Reynolds number of $2.1 \cdot 10^4$, the free stream velocity U_∞ is equal to 10.3 m/s while the cylinder diameter is $3 \cdot 10^{-2}$ m. The reported baseline drag coefficient value is in alignment with the results described in the study conducted by Cheng et al. [16].

An uncertainty analysis has been carried out on the experimental data for the uncontrolled drag coefficient to validate the repeatability of the experiments. The method for the error estimation developed by Moffat [17] gave an estimated error for the drag coefficient of around 1.5 %, considering an uncertainty of 0.03 % on of the full-scale for each load cell and an uncertainty of 1.5 % of the measured value for the differential pressure transducer used.

Before starting the investigation based on the gMLC algorithm, a parametric investigation on the same experimental environment has been performed. Such an analysis had the the aim of identifying the optimal actuation parameters, i.e. frequency, duty cycle and amplitude, values starting from a sinusoidal waveshape widely used in literature. It was found that the optimal waveshape was characterized by an actuation frequency of around 88 Hz. For this reason, in the later investigations, the starting population of analytical functions

consists of 12 harmonic functions, which are the 1st- to the 6th- order harmonics with a fundamental frequency of 44 Hz and the algorithm combines these laws using several operations (sum, difference and multiplication) and mathematical operators (sine and cosine).

Figure 3 illustrates the learning process of gMLC algorithm for the aerodynamic drag reduction of a circular cylinder by reporting the trend of the cost function with respect to the number of tested individuals (left panel) and the optimal waveshape of the voltage input signal (corresponding to the individual with the minimum cost) compared to a sinusoidal signal with the same frequency and amplitude.

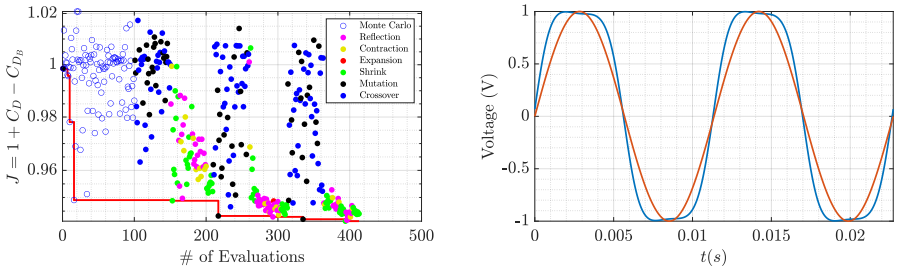

Fig. 3 Left: Distribution of the costs during the gMLC optimization process; right: waveshape of the best individual voltage control law found via the gMLC algorithm (blue curve) compared with the sinusoidal one (orange curve).

In the left panel, the trend of the cost function J with respect to the number of individuals is reported. We notice that in the first exploration phase, individuals $i = 101, \ldots, 150$ show a similar cost value compared with the Monte Carlo phase-generated individuals. In the following exploitation, the individuals with $i = 151, \ldots, 200$ presents a descent, improving the best solution compared with the previous exploration phase. During this phase, we notice a clear trend for the cost of the new individuals that indicates that the simplex is going down towards a minimum. This descent is interrupted by the next exploration phase. Individuals $i = 201, \ldots, 250$ greatly improve the best solution, finding an individual having a much lower cost than those in the simplex. The next exploitation phase brings to a new improvement in terms of the cost function, reaching a new minimum, while the next exploration phase gives good individuals that have been included in the simplex. After 350 evaluations, major improvements are performed by exploitation phases. In fact, last exploitation phase of the experiment reports a final steep descent characterized by a new minimum value of the cost function J equivalent to 0.941, which corresponds to a drag coefficient value associated to this control law equivalent to 0.86; this has been considered as the best actuation law found by gMLC procedure.

The percentage drag reduction with respect to the uncontrolled configuration is estimated to be around 7.6 % for the best individual found by gMLC algorithm. To validate the goodness of the actuation law obtained by Machine

Learning, a sinusoidal waveshape, characterized by an actuation frequency equals to 88 Hz and an amplitude of 1 V, has been tested and the relative percentage drag reduction law has been measured. The latter is reported to be equivalent to 6.1 % with respect to baseline configuration, confirming the increase of drag reduction obtained via gMLC procedure, which attests to 1.5 % with respect to sinusoidal control law.

Right panel of Figure 3 reports the comparison between the just mentioned control laws, showing that the gMLC algorithm has been able to obtain a very complex actuation law which is characterized by a suction duty cycle d very close to 0.5, typical of a sinusoidal waveshape. On the other hand, the effect of gMLC algorithm in our study seems to be concentrated on the shape of the signal rather than on the suction duty cycle, but it can be observed that the combination of individuals of the same generation can generate control laws characterized by a duty cycle different from 0.5. In this study, both in the ejection and suction phase, gMLC-based control law seems to tend to a square wave, compared to a classical sinusoidal waveshape.

5.2 PIV measurements

The results of the planar PIV investigation of the flow field downstream the circular cylinder are here reported and discussed. Three different configurations have been tested: the uncontrolled one, the controlled configuration with a sinusoidal waveshape characterized by an actuation frequency of 88 Hz and the flow field generated by the interaction between the optimal actuation law found via gMLC algorithm and the von Karman street. 2-D component PIV measurements are performed with an acquisition frequency of 10 Hz corresponding to a sequence of 6000 snapshots for the cases studied.

5.2.1 Structure of the flow field

Figure 4 (a), (b) and (c) reports the time-averaged flow fields, in terms of the streamwise velocity component $\bar{u}$ with superimposed streamlines for all the configurations studied, uncontrolled and controlled.

Natural case, Figure 4 (a), reports the classic flow field morphology characterized by an extended recirculation region behind the cylinder [2, 18]. Such a zone is delimited by two elongated shear layers ending with two counter-rotating vortex structures representative of the time-averaged behaviour and position of the shed von Kármán vortices. The large recirculation region emerges where the backward flow is behind the circular cylinder and a large velocity defect is reported in the near-wake region of the circular cylinder due to the flow separation for the natural case. The extent of this recirculation region, delimited by the presence of a saddle point, is approximately $2D$, where D is the diameter of the circular cylinder, in agreement with the study by Zouh et al. [19].

Both the studied controlled configurations, reported in Figure 4 (b) and (c), show an additional vortex pair in the flow field with respect to the baseline case;

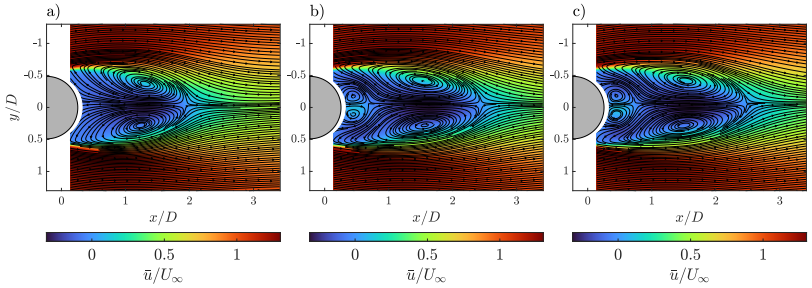

Fig. 4 Time-averaged streamwise velocity component with superimposed streamlines for three configurations: (a) baseline case, (b) controlled configuration with sinusoidal wave-shape, (c) controlled configuration found via gMLC algorithm.

this is the time-averaged footprint of the issued synthetic jet. Furthermore, the vortex pair has a circulation opposite to that of the von Kármán vortices and a peak of streamwise velocity can be detected and it is linked to the injection of momentum in that region. The simultaneous presence of these two structures results in an additional time-averaged saddle point located at around $0.67D$ from the cylinder centre, for the case (b), and around $0.73D$ for the case (c).

An analysis made to better understand turbulent statistics of the phenomenon is here shown in Figure 5, where the maps of the dimensionless Turbulent Kinetic Energy (TKE), calculated as $0.5\left(\overline{u'u'}/U_\infty^2 + \overline{v'v'}/U_\infty^2\right)$ and associated to the vortex structures is reported; typycally, TKE is used as a measurement of the turbulence mixing [20, 21]. From Figure 5, it can be inferred that the synthetic jet can enhance the TKE in the near wake for $x/D \leq 1.5$, and the increment is different considering the two different controlled configurations, whereas the TKE decreases for $x/D \geq 1.5$. The production of the TKE can be related to the dynamics of the vortices. The reduction of TKE in the part where the shedding vortices come off suggests a reduction of the shedding phenomenon itself. This is accompanied by an increase of TKE in the nearby wake, due to the dynamics of the synthetic jet. From this point of view, the configuration found with gMLC algorithm is certainly better.

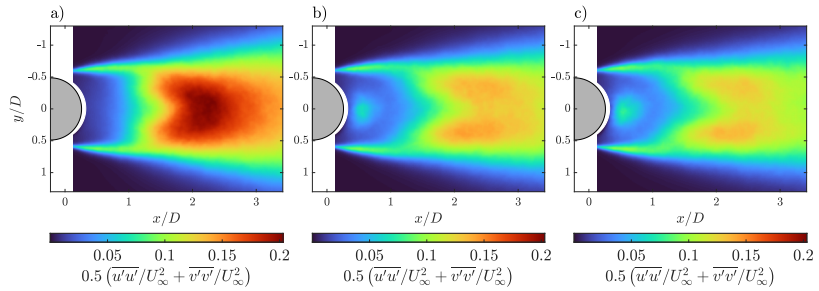

Fig. 5 Dimensionless Turbulent Kinetic Energy $0.5\left(\overline{u'u'}/U_\infty^2 + \overline{v'v'}/U_\infty^2\right)$' maps for three configurations: (a) baseline case, (b) controlled configuration with sinusoidal waveshape, (c) controlled configuration found via gMLC algorithm.

Also for the gMLC control law configuration, the synthetic-jet vortices, located near the rear of the circular cylinder, influence the flow field. The synthetic jet can thus enhance the turbulence mixing in the near wake. In contrast, the control with a sinusoidal waveshape is also dominated by the presence of the footprint of the synthetic jet actuation but with lower values near the rear stagnation point. This result is also confirmed in the maps of the streamwise-normal components of the Reynolds stress tensor for the three configurations analyzed, reported in Figure 6. In fact, a difference between the two controlled configurations emerges in terms of intensity of dimensionless streamwise-normal Reynolds stress where the footprint of the synthetic jet is located. An higher value of normal Reynolds stress can be experienced in the case *c* with respect to the sinusoidal waveshape, with an increase of 14 % between these two cases. This trend emerges also in the shear layers, with a trend of increasing intensity of normal-streamwise Reynolds stress which leads to an increase around 18 % between the two cases. It should also be noted that normal stresses in the centre of von Karman vortices are greater in the baseline case than in the controlled ones.

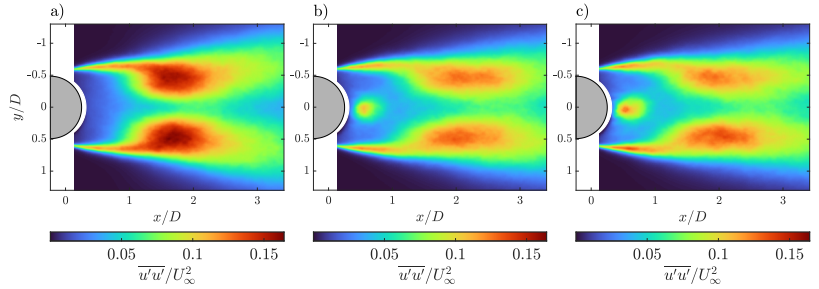

Fig. 6 Dimensionless streamwise-normal Reynolds stress $\overline{u'u'}/u_\infty^2$ maps for : (a) baseline case, (b) controlled configuration with sinusoidal waveshape, (c) controlled configuration found via gMLC algorithm.

5.3 POD Analysis

In order to better understand the physical phenomenon, a modal decomposition of the velocity field obtained by PIV technique has been undertaken. In the following, the application of Proper Orthogonal Decomposition (POD) to the raw data obtain via PIV for the three analyzed configurations would be discussed. Works by Ma et al. [22] and Perrin et al. [23] reported that only the first two modes are needed to reconstruct the natural vortex shedding process, while in this study the first four modes have been used to identify eventual characteristic structures of the flow-field for all the configurations tested. Since it is found that the first two modes can represent the natural Karman vortex shedding process, the third and fourth modes can represent the characteristic of the synthetic jet for both the controlled cases. However, they are already enough to present the dominant vortex shedding characteristic for all cases.

Figure 7 reports the percentage of the cumulative POD modes energy to the total one and the percentage of the energy fraction associated to the first ten POD modes. It is indicated that the first few modes occupy most of the energy for all cases, while the energy percentage for higher mode decreases to zero gradually and this trend can be inferred from the Fig. 7 (*a*).

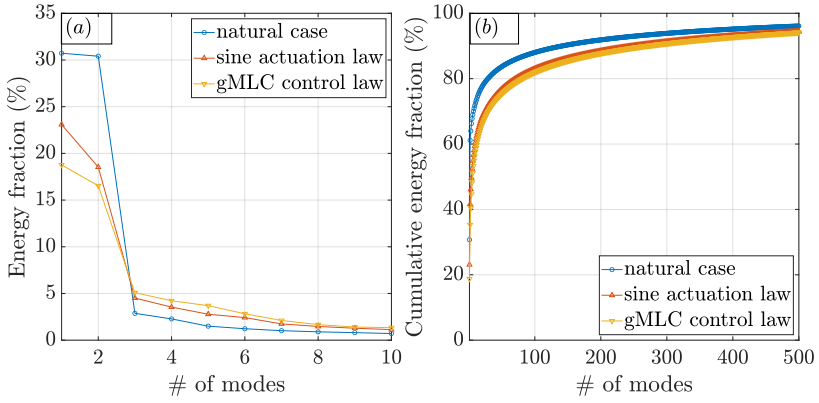

Fig. 7 Percentage of the cumulative POD modes energy to the total modes energy at $Re = 2 \cdot 10^4$ for the three configurations investigated: baseline (blue dots), sinusoidal waveshape (red triangles) and optimal waveshape from gMLC (yellow triangles).

Figure 8 shows the first four POD modes for the time-averaged streamwise velocity component related to the natural case. In the first and second mode, the same structure emerges for all modes, which is anti-symmetrical to the x-axis and represents the translational movement of structures in the flow; this pattern is also reported in literature in the work by Brevis and García-Villalba [24]. It is noteworthy to observe that by virtue of the modal decomposition, symmetrical distributions about the x-axis actually represent anti-symmetrical spatio-temporal flow features whereas those distributions with reflected symmetry, i.e., having opposite sign about the x-axis, correspond to symmetrical

flow features. Modes 1 and 2 in the uncontrolled configuration exhibit similar spatial distributions but shifted in the streamwise direction and they are linked to the spatio-temporal pattern of a traveling wave formed as vortices shed from alternates sides of the cylinder are convected downstream. Modes 3 and 4 instead can have a dubious physical interpretation. Mode 3 is concentrated in the separating shear layers and near the end of the vortex formation region; this mode might be linked to the Bloor–Gerrard shear-layer instability which is a well-established feature of turbulent cylinder wakes for Reynolds numbers above few hundred [25]. On the other hand, mode 4 is not clearly defined and this makes it hard to infer its physical origin, if it is not an artifact of the modal decomposition.

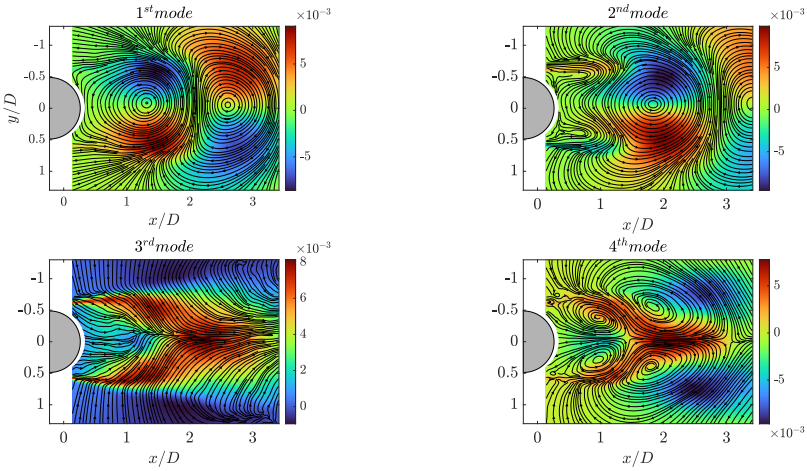

Fig. 8 The first four POD modes in the uncontrolled configuration at $Re = 2 \cdot 10^4$ for the fluctuating streamwise velocity component.

Figures 9 and 10 report instead the first four POD modes associated to the two controlled configurations tested: sinusoidal one and the optimal control law found via gMLC algorithm. As expected, first two modes for both the controlled cases are like half-arrowhead structures antisymmetric about the centerline, which are similar with those of the natural case reported in Figure 8 while modes 3 and 4 are quite different compared with the natural case. Despite the similarity of the modal distributions in the natural and controlled wake, the contour levels are an order of magnitude higher in the case of gMLC control law with respect to natural case. Mode 3 distributions appear somewhat different in the forced wake than those in the natural case. The fourth mode exhibits rather well-defined distributions in the forced wake which are substantially different than the corresponding ones in the natural case indicating that this mode is associated with different flow features linked to the synthetic jet interaction with the ambient fluid.

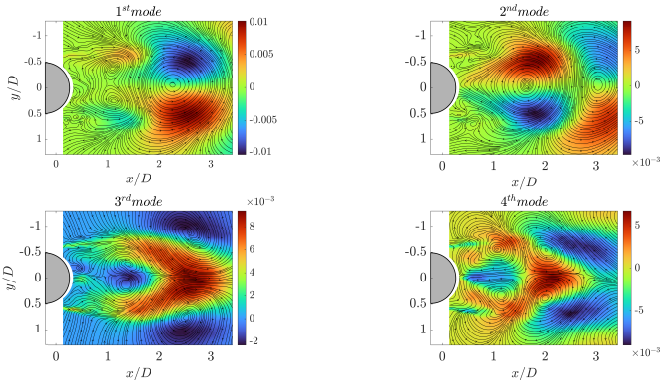

Fig. 9 The first four POD modes for the sinusoidal controlled configuration at $Re = 2 \cdot 10^4$ for the fluctuating streamwise velocity component.

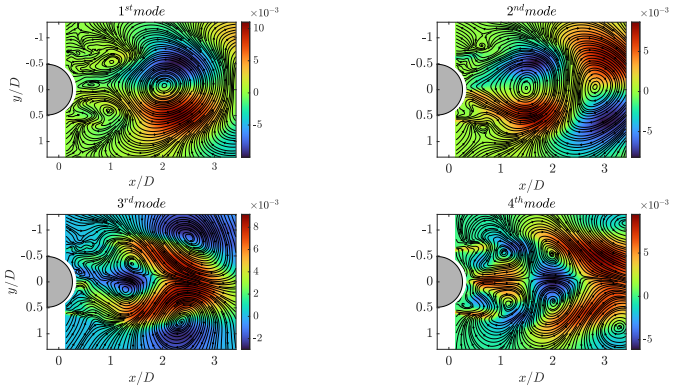

Fig. 10 The first four POD modes for the gMLC controlled configuration at $Re = 2 \cdot 10^4$ for the fluctuating streamwise velocity component.

6 Conclusions

In this paper, we present an application of linear genetic programming control (LGPC) to an open loop active flow control of the wake of a circular cylinder to reduce the associated aerodynamic drag. The flow has been manipulated via a Synthetic Jet actuator located at the rear stagnation point on the surface of the test article, i.e. the circular cylinder. Moreover, once obtained the optimal control law found via gMLC algorithm, an investigation using Particle Image Velocimetry technique has been performed to investigate the mean flow quantities and turbulent statistics of the phenomenon and to observe differences and analogies between controlled and uncontrolled configurations. Additionally, a modal decomposition based on the PIV input data is performed to highlight the structures of the flow field.

First, the linear genetic programming has proved to be an efficient computational tool for the active control of the wake flow downstream of a circular

cylinder. In fact, optimal waveshape found via gMLC algorithm demonstrated its efficiency in reducing properly the aerodynamic drag with respect to natural case better than the sinusoidal waveshape tested. The gMLC control law is able to give a percentage drag reduction equals to 7.6 % with respect to natural case, while the sinusoidal control law gives a percentage drag reduction equals to 6.1 %; the LGPC-based control law confirms the goodness of the optimization procedure giving an increase of 1.5 % of the drag reduction compared with the sinusoidal waveshape. Moreover, the control law found via gMLC has solved the issue linked to the *a priori* imposition of a specific waveshape. In fact, gMLC algorithm is able to solve the optimization problem finding an optimal control law whose mathematical expression can be obtained and physically interpreted.

Second, Particle Image Velocimetry measurements allow to understand the fluid dynamic configurations showing similarities and differences with respect to baseline case. Controlled cases report the classic footprint of the synthetic jet actuation characterized by two counter-rotating vortices with an opposite circulation with respect to the von Karman shed vortices and the appearance of a second saddle point in the flow field with a moving of the primary saddle point characteristic of the baseline configuration. gMLC-based actuation reports higher values of the normal Reynolds stresses in the shear layers and where the footprint of the synthetic jet is located with respect to sine controlled actuation. Velocity fluctuations in the wake are also reduced for the gMLC control law compared with the sinusoidal waveshape and this implies a better suppression of vortex shedding; this trend can be inferred from TKE distributions. Except for these differences, the two controlled configurations exhibit a similar structure of the flow fields.

POD analysis allowed to have a better understand of the effect of the interaction between the SJ and the cylinder's wake focusing on the differences between the three tested configurations. In fact, the uncontrolled configuration exhibits a larger energetic content of the first couple of POD modes compared to the controlled configurations. The actuation of the SJ generates a decreasing of the percentage energy fraction corresponding to a specific mode depending from the reduction of the scale of the dominant coherent structures of the flow fields for both the controlled cases. The analysis of the first four POD modes for the controlled cases reports instead a similarity for the first couple of POD modes between the controlled and uncontrolled configurations, while modes 3 and 4 are quite different compared with the natural case. The contour levels are an order of magnitude higher in the case of gMLC control law with respect to the uncontrolled configuration and the fourth mode shows distributions in the forced wake which are associated with the interaction between the SJ and the ambient fluid.

References

[1] Wiliamson, C.: Vortex dynamics in the cylinder wake (1996)

[2] Greco, C.S., Paolillo, G., Astarita, T., Cardone, G.: The von kármán street behind a circular cylinder: Flow control through synthetic jet placed at the rear stagnation point. Journal of Fluid Mechanics **901** (2020)

[3] Seifert, A., Bachar, T., Koss, D., Shepshelovich, M., Wygnanski, I.: Oscillatory blowing: a tool to delay boundary-layer separation. AIAA journal **31**(11), 2052–2060 (1993)

[4] Feng, L.H., Wang, J.J.: Circular cylinder vortex-synchronization control with a synthetic jet positioned at the rear stagnation point. Journal of Fluid Mechanics **662**, 232–259 (2010)

[5] Feng, L.-H., Wang, J.-J.: Synthetic jet control of separation in the flow over a circular cylinder. Experiments in fluids **53**(2), 467–480 (2012)

[6] Maceda, G.Y.C., Li, Y., Lusseyran, F., Morzyński, M., Noack, B.R.: Stabilization of the fluidic pinball with gradient-enriched machine learning control. Journal of Fluid Mechanics **917** (2021)

[7] Rowan, T.: The subplex method for unconstrained optimization. PhD thesis, Department of Computer Sciences, University of Texas (1990)

[8] Duriez, T., Brunton, S.L., Noack, B.R.: Machine Learning Control-taming Nonlinear Dynamics and Turbulence vol. 116. Springer, ??? (2017)

[9] Astarita, T.: Analysis of weighting windows for image deformation methods in piv. Experiments in fluids **43**(6), 859–872 (2007)

[10] Astarita, T.: Analysis of velocity interpolation schemes for image deformation methods in piv. Experiments in Fluids **45**(2), 257–266 (2008)

[11] Berkooz, G., Holmes, P., Lumley, J.L.: The proper orthogonal decomposition in the analysis of turbulent flows. Annual review of fluid mechanics **25**(1), 539–575 (1993)

[12] Taira, K., Brunton, S.L., Dawson, S.T., Rowley, C.W., Colonius, T., McKeon, B.J., Schmidt, O.T., Gordeyev, S., Theofilis, V., Ukeiley, L.S.: Modal analysis of fluid flows: An overview. Aiaa Journal **55**(12), 4013–4041 (2017)

[13] Lumley, J.L.: The structure of inhomogeneous turbulent flows. Atmospheric turbulence and radio wave propagation, 166–178 (1967)

[14] Volkwein, S.: Proper orthogonal decomposition: Theory and reduced-order modelling. Lecture Notes, University of Konstanz **4**(4), 1–29 (2013)

[15] Sirovich, L.: Turbulence and the dynamics of coherent structures. i. coherent structures. Quarterly of applied mathematics **45**(3), 561–571 (1987)

[16] Cheng, N.-S., *et al.*: Calculation of drag coefficient for arrays of emergent circular cylinders with pseudofluid model. Journal of Hydraulic Engineering **139**(6), 602–611 (2013)

[17] Moffat, R.J.: Describing the uncertainties in experimental results. Experimental thermal and fluid science **1**(1), 3–17 (1988)

[18] Feng, L.H., Wang, J.J., Pan, C.: Effect of novel synthetic jet on wake vortex shedding modes of a circular cylinder. Journal of Fluids and Structures **26**(6), 900–917 (2010)

[19] Zhou, B., Wang, X., Gho, W.M., Tan, S.K.: Force and flow characteristics of a circular cylinder with uniform surface roughness at subcritical reynolds numbers. Applied Ocean Research **49**, 20–26 (2015)

[20] Benard, N., Balcon, N., Touchard, G., Moreau, E.: Control of diffuser jet flow: turbulent kinetic energy and jet spreading enhancements assisted by a non-thermal plasma discharge. Experiments in fluids **45**(2), 333–355 (2008)

[21] Schäfer, F., Breuer, M., Durst, F.: The dynamics of the transitional flow over a backward-facing step. Journal of Fluid Mechanics **623**, 85–119 (2009)

[22] Ma, X., Karamanos, G.-S., Karniadakis, G.: Dynamics and low-dimensionality of a turbulent near wake. Journal of fluid mechanics **410**, 29–65 (2000)

[23] Perrin, R., Braza, M., Cid, E., Cazin, S., Barthet, A., Sevrain, A., Mockett, C., Thiele, F.: Obtaining phase averaged turbulence properties in the near wake of a circular cylinder at high reynolds number using pod. Experiments in Fluids **43**(2), 341–355 (2007)

[24] Brevis, W., García-Villalba, M.: Shallow-flow visualization analysis by proper orthogonal decomposition. Journal of Hydraulic Research **49**(5), 586–594 (2011)

[25] Feng, L.-H., Wang, J.-J., Pan, C.: Proper orthogonal decomposition analysis of vortex dynamics of a circular cylinder under synthetic jet control.

Physics of Fluids **23**(1), 014106 (2011)